High Temperature Corrosion of Materials (2025) 102:2
https://doi.org/10.1007/s11085-024-10324-0

RESEARCH

Influence of the Cooling Rate on the Wüstite Content in Oxide Layers Formed During High-Temperature Oxidation of Hot-Worked Tool Steel with High Thermal Conductivity

Tilen Balaško[1] · Barbara Šetina Batič[2] · Jaka Burja[1,2]

Received: 18 September 2024 / Revised: 18 October 2024 / Accepted: 25 October 2024

Abstract

The transformation of wüstite (FeO) in the oxide layer formed during high temperature oxidation (600 °C and 700 °C) on hot-worked tool steel was investigated. Wüstite plays an important role in the oxide layer of these steels used for hot working. However, understanding its transformation behavior during cooling is crucial for controlling the final oxide layer structure. Slow cooling rates have a significant influence on the final wüstite content, resulting in inaccurate representations of the composition of the oxide layer at temperatures above 570 °C. The aim of this study was to determine the influence of cooling rate on the wüstite content in the oxide layer after high temperature oxidation. It was found that for hot-worked steel samples oxidized at 700 °C or higher, a cooling rate of more than 1000 °C min^{-1} is required to suppress the eutectoid transformation and maintain the realistic wüstite content. At lower temperatures (570 °C–600 °C), a cooling rate of more than 100 °C min^{-1} is required to achieve the wüstite content observed at oxidation temperatures in the oxide layer. Overall, the hematite and magnetite contents also vart with the cooling rate, which is associated with changes in the wüstite content.

Keywords High-temperature oxidation · Oxide layer · Wüstite · Hot-work tool steel · CALPHAD

✉ Tilen Balaško
tilen.balasko@ntf.uni-lj.si

[1] Faculty of Natural Sciences and Engineering, University of Ljubljana, Aškerčeva cesta 12, 1000 Ljubljana, Slovenia

[2] Institute of Metals and Technology, Lepi pot 11, 1000 Ljubljana, Slovenia

Published online: 28 November 2024

Introduction

The production of hot-worked tool steels to achieve the desired mechanical properties and final shapes requires a combination of processes: forging, rolling, heat treatment and machining. Both forging and rolling are carried out at elevated temperatures, usually in air [1–3]. Heat treatment, on the other hand, can be divided into two stages: (1) heat treatment during the manufacturing process and (2) final heat treatment, which usually occurs after machining. However, in the final heat treatment, a protective atmosphere is usually used to minimize oxidation [1, 3–7]. Therefore, the formation of an oxide layer during forging, rolling and the first heat treatment stage is unavoidable. When these processes take place above 570 °C, wüstite (FeO) becomes thermodynamically stable [8–12]. Consequently, it forms and usually dominates the oxide layer, with the overall oxide growth rate being determined by the FeO growth rate [11–16]. Furthermore, from an end-user perspective, hot work tool steels are mainly used for high temperature applications (extrusion, die casting, hot forging, rolling, etc.), with some even exceeding 570 °C [1, 4, 17]. Therefore, understanding the eutectoid transformation behavior, which refers to the degradation of the wüstite during cooling, is crucial as it influences the final structure of the oxide layer [18, 19].

When it comes to the high-temperature oxidation of steels, the focus on the Fe–O system is crucial. This system comprises three main types of oxides: wüstite (FeO), magnetite (Fe_3O_4) and hematite (Fe_2O_3) [8, 10, 13, 20]. Wüstite (FeO) is a p-type oxide with a non-stoichiometric character, i.e. its composition can vary considerably (δ can reach 0.15, resulting in a stoichiometry of $Fe_{0.95}O$ to $Fe_{0.85}O$). Interestingly, the self-diffusion of oxygen in wüstite is much slower than the self-diffusion of iron [9, 10, 12, 21]. Magnetite (Fe_3O_4) is an inverse spinel structure with divalent Fe^{2+} ions in octahedral sites and half of the trivalent Fe^{3+} ions in tetrahedral sites. Unlike at high temperatures, magnetite shows only a minimal deviation from stoichiometry [9, 12, 14, 21]. Hematite (Fe_2O_3) shares a crystal structure with Cr_2O_3 and α-Al_2O_3 and exhibits a corundum structure. It is classified as an n-type oxide with minimal stoichiometric deviation [9, 12, 21]. Therefore, the oxide layer that forms on pure Fe above 570 °C consists of three different sublayers: Wüstite, magnetite and hematite. Interestingly, the layer thickness is largely independent of the temperature. Moreover, diffusion is much faster in wüstite (which accounts for about 95% of the total oxide layer thickness) than in magnetite (4%) and hematite (1%) [9, 13, 15, 21]. Studies by Himmel, Mehl and Birchenall [22] found that iron ion diffusion dominates in the $Fe_{1-\delta}O$ and Fe_3O_4 sublayers, based on measurements of the self-diffusion coefficient of iron in these oxides. Conversely, oxygen diffusion takes precedence in Fe_2O_3 [11]. This rapid diffusion of reactants within wüstite, which is favored by the large number of voids, is a key factor in iron oxidation [23].

In the case of wüstite, we know that the amount that remains in the oxide layer after high-temperature oxidation (above 570 °C) depends on how quickly it cools. The slower the cooling rate, the more wüstite decomposes into magnetite and iron [13, 19, 24–26]. Gleeson et al. [27] have studied this phenomenon in detail and

even produced a transformation diagram for the FeO oxide layer on mild steel at 900 °C in air. Based on previous studies on the eutectoid transformation of the wüstite layer on low-carbon steel [28], this decomposition appears to occur in two stages:

$$(1-4y)Fe_{1-x}O \rightarrow (1-4x)Fe_{1-y}O + (x-y)Fe_3O_4 \tag{1}$$

$$x > y$$

$$4Fe_{1-y}O(ironrich) \rightarrow Fe_3O_4 + (1-4y)\alpha - Fe \tag{2}$$

There was also a study on the effects of the initial scale structure on the transformation behavior of wüstite by Tanei et al. [26]. It was found that the phase transformation of wüstite can be controlled by the initial scale structure.

So far, no research has looked at how wüstite transforms in hot-work tool steels. Remember that these steels are used at high temperatures and that even the forming process of the steels takes place at temperatures above the A_3 point. Furthermore, the cooling rates during these processes are usually not controlled. Therefore, we decided to investigate how different cooling rates affect the amount of wüstite remaining in the oxide layer formed on our hot-work tool steel after high-temperature oxidation at 600 °C and 700 °C. The actual oxide layer on the Mo–W–Ni steel and its composition have already been studied in detail [29], so we focused specifically on how the wüstite decomposes at different cooling rates (known as eutectoid transformation). In this study, the effect of cooling rate on the amount of wüstite remaining in the oxide layer that forms on hot-work tool steels after 24 h of oxidation at high temperatures is investigated. Although there are many studies on high temperature oxidation, the cooling rates are often either unknown or too slow (above 570 °C). This has a significant impact on the final wüstite content and leads to inaccurate representations of the composition of the oxide layer that forms at temperatures above 570 °C.

Experimental Procedures

In this study, the influence of the cooling rate on the decomposition, also called eutectoid transformation, of wüstite on Mo–W–Ni hot work tool steel with high thermal conductivity after high temperature oxidation was investigated. A combination of wet chemical analysis and post-combustion infrared absorption with

Table 1 Chemical composition of the analyzed Mo-W–NI steel given in wt%

C	Si	Mn	P	S	Cu	Cr	Mo	Ni	Al	W	Fe
0.32	0.12	0.23	0.005	0.001	0.01	0.11	3.20	2.10	0.01	1.90	Bal

ELTRA CS-800 was used to determine the chemical composition of the steel. The detailed results are shown in Table 1.

The influence of the cooling rate on the wüstite content in the oxide layer formed on hot work tool steel with high thermal conductivity was investigated. The samples were subjected to high-temperature oxidation at 600 °C and 700 °C for 24 h in dry air. Five different cooling rates (1 °C min^{-1}, 10 °C min^{-1}, 100 °C min^{-1} and 1000 °C min^{-1}) were used to evaluate their effects. Prior to oxidation, the steel was soft annealed at 850 °C for 4 h, followed by controlled cooling in the furnace (15 °C h^{-1}) to 600 °C and room temperature. The samples with dimensions h = 4 mm and Φ = 4 mm were then prepared for oxidation. Slow cooling rates (1 °C min^{-1} and 10 °C min^{-1}) were achieved using a NETZSCH STA Jupiter 449C instrument, while higher rates (100 °C min^{-1} and 1000 °C min^{-1}) were enabled by a TA Instruments DIL-805A/D instrument. Both devices were operated with air (79 vol% N_2, 21 vol% O_2, 0.9 vol% Ar_2, 0.1 vol% hydrocarbons and inert gasses) flowing at 30 mL min^{-1}.

The samples were ground and polished to prepare them for a detailed analysis of their microstructure. This analysis was carried out using a scanning electron microscope (JEOL JSM 6450-F), which revealed the overall structure of the material. In addition, energy dispersive spectroscopy (EDS) and electron backscatter diffraction (EBSD) provided further insight into the elemental composition and crystallographic orientation of the different phases present in the microstructure.

The Thermo-Calc software (version 2023b) was used to perform the CALPHAD calculations. In particular, the Metal Oxide Solutions Database (TCOX12) provided the necessary thermodynamic data to predict the theoretical equilibrium composition of the oxide layers formed. The calculations were performed in console mode, where O can be set as gas (O_2). The results show the composition of the oxide layer as a function of the activity of the O_2 formed on the analyzed steel at the investigated oxidation temperatures.

Results

CALPHAD Calculations

In order to gain an initial understanding of the composition of the oxide layer at different oxygen activities (a_{O_2}), we have calculated the theoretical equilibrium composition at both oxidation temperatures (600 °C and 700 °C). These calculations are shown in Figs. 1 and 2, where the amount of each phase (in wt%) within the oxide layer varies as a function of a_{O_2}. Since a_{O_2} has low values, it may be equal to the partial pressure of O_2 due to thermodynamics. When this is taken into account, the results of the calculations show the equilibrium composition of the oxide layer from the atmosphere (higher a_{O_2}) to the steel surface (lower a_{O_2}). It is important to note that we used a new database (TCOX12) for these calculations, which has led to some differences compared to previously published results [29]. These discrepancies are the reason why we included this analysis, and we will discuss them later on.

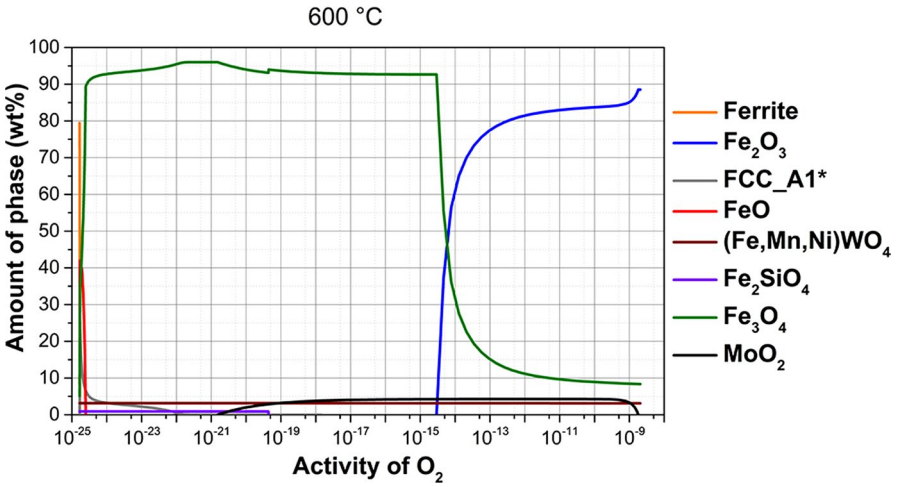

Fig. 1 Calculated composition of the oxide layer that forms at an oxidation temperature of 600 °C

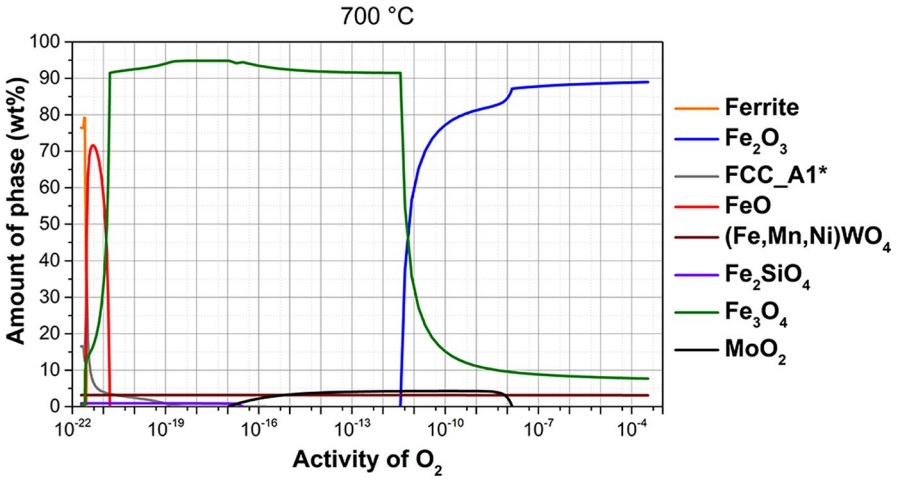

Fig. 2 Calculated composition of the oxide layer that forms at an oxidation temperature of 700 °C

It can be seen from Fig. 1 that the oxide layer formed at 600 °C can be divided into three sublayers based on oxygen activity (a_{O_2}). The outer oxide sublayer ($a_{O_2} \approx 10^{-9}$ to 10^{-14}) is dominated by Fe_2O_3 and gradually transitions to Fe_3O_4 as we move inward (from ~ 88.9 wt% Fe_2O_3 to 0 wt%, and ~ 8.6 wt% Fe_3O_4 to ~ 92.6 wt%, respectively). Small amounts of MoO_2 (~ 4.6 wt%) and (Fe,Mn,Ni)WO_4 (~ 3.5 wt%) are also present here. Below $a_{O_2} \approx 10^{-15}$, a middle oxide sublayer is formed, consisting mainly of Fe_3O_4 (~ 92.6 wt% – ~ 96.4 wt%) with the same low MoO_2 and (Fe,Mn,Ni)WO_4 phases. At $a_{O_2} \approx 10^{-19}$, Fe_2SiO_4 (~ 1.2 wt%) enters the middle oxide sublayer, followed by FCC_A1* (~ 2.6 wt%) at $a_{O_2} \approx 10^{-22}$. This FCC_A1* is essentially

Ni enriched ferrite (as Ni is a gamma stabilizing element), but the software misinterprets it as austenite (this is clarified and explained below using SEM analyzes, particularly EBSD, where it is shown to be essentially ferrite with increased Ni content). Finally, below $a_{O_2} \approx 10^{-24}$ the inner oxide sublayer is formed. Here, FeO (up to 40.4 wt% at the steel interface) and Fe_3O_4 (decreasing towards the interface to ~ 5.4 wt%) are the main players, accompanied by small amounts of (Fe,Mn,Ni)WO_4, Fe_2SiO_4 and FCC_A1* (their content increases to ~ 25.9 wt% at the boundary between steel and inner oxide sublayer).

At 700 °C, Fig. 2 shows a similar oxide layer structure to that at 600 °C, but with some important differences. The outer oxide sublayer ($a_{O_2} \approx 10^{-4}$ to 10^{-11}), again dominated by Fe_2O_3 and transitioning inward to Fe_3O_4, has a slightly higher Fe_2O_3 content initially (the further we go to the center, the less Fe_2O_3 is present, from ~ 89.2 wt% to 0 wt%). MoO_2 and (Fe,Mn,Ni)WO_4 remain present at ~ 4.5 wt% and ~ 3.5 wt%, respectively. The middle oxide sublayer (a_{O_2} below 10^{-11}) consists mainly of Fe_3O_4 (~ 92.1 wt% – ~ 95.1 wt%) with the same minor MoO_2 (~ 4.7 wt%) and (Fe,Mn,Ni)WO_4 (~ 3.4 wt%) phases. However, Fe_2SiO_4 and FCC_A1* appear earlier here: Fe_2SiO_4 (~ 1.2 wt%) occurs at $a_{O_2} \approx 10^{-16}$, followed by FCC_A1* with a wider range (~ 0.05 wt% to ~ 3.5 wt%). Finally, the inner oxide sublayer (a_{O_2} below 10^{-20}) shows a significant difference. While FeO becomes the dominant phase (up to ~ 72.0 wt% at the interface), its initial presence and higher overall content compared to 600 °C are noteworthy. Fe_3O_4 still decreases towards the interface but remains predominant (~ 46.6 wt% to ~ 12.7 wt%). Slightly more (Fe,Mn,Ni)WO_4 (~ 3.2 wt%), Fe_2SiO_4 (~ 1.0 wt%) and FCC_A1* are present, with FCC_A1* reaching a much higher concentration of ~ 39.7 wt% at the interface.

According to the calculations, both oxidation temperatures (600 °C and 700 °C) have similar oxide layer structures. The outermost oxide sublayer consists mainly of Fe_2O_3 with some Fe_3O_4, accompanied by small amounts of MoO_2 and (Fe,Mn,Ni)WO_4. The middle oxide sublayer consists mainly of Fe_3O_4 with additional MoO_2, (Fe,Mn,Ni)WO_4, Fe_2SiO_4 and FCC_A1*, which consists mainly of Ni enriched ferrite. Finally, the inner oxide sublayer is dominated by FeO and Fe_3O_4, together with small amounts of (Fe,Mn,Ni)WO_4, Fe_2SiO_4 and FCC_A1* (Ni enriched ferrite). The decisive difference in the composition of the oxide layer lies in the amount of wüstite in the inner sublayer. At 600 °C, the inner sublayer contains around 40 wt% wüstite, while at 700 °C this value rises to around 70 wt%.

Scanning electron microscopy (SEM) with EBSD analysis is used to quantify the total wüstite content. We expect samples oxidized at 700 °C to have a higher wüstite content at cooling rate of 1000 °C min^{-1}. However, at lower cooling rates, the final wüstite content depends on the extent of its transformation (eutectoid transformation) to magnetite.

Scanning Electron Microscopy

Since the thickness and composition of the oxide layers had already been measured previously [29], this study focused exclusively on their composition at different cooling rates. Table 1 shows the results of the percentage of oxides for each

sample studied. The results were as expected, i.e. the higher the cooling rate, the more wüstite should be retained in the oxide layer. This proves the importance of the cooling rate for the composition of the oxide layer. At higher oxidation temperatures (700 °C), the proportion of wüstite in the oxide layer is also higher. Even at a cooling rate of 1 °C min^{-1} the proportion of wüstite is higher than at an oxidation temperature of 600 °C and a cooling rate of 1000 °C min^{-1} (Table 2).

In all the following figures (Figs. 3, 4, 5, 6, 7), the oxide layer was divided into three sub-layers: 1—outer oxide sub-layer, 2—middle oxide sub-layer and 3—inner oxide sub-layer. The steel (substrate) has also been labeled in the following figures.

Figure 3 shows the inner oxide sublayer of the sample oxidized at 600 °C and cooled at a cooling rate of 1 °C min^{-1}. An SEM image of the analyzed oxide sublayer with the corresponding results of EBSD phase analysis, EDS analysis of the surface distribution of elements and crystal orientations. This analysis was performed to prove that there are ferrite islands in the inner oxide sublayer, which was also predicted by the calculations of the CALPHAD method. The ferrite remains are present in all samples analyzed, but the total fraction influences the wüstite fractions. As they have the same crystal structure (BCC—body-centered cubic), it is not analyzed further. However, to show how to distinguish between them, an EDS elemental analysis was performed. Ferritic remains have a higher Ni content and a lower O content, which was already observed in the CALPHAD calculation results. These ferritic remains were also the reason that EBSD analysis was used to calculate the fraction of oxides in the oxide layers formed, as we were able to distinguish them from wüstite based on Ni content, as previously mentioned. This provided more accurate results regarding the amount of each oxide in the oxide layers.

Figure 4 shows an SEM image of the analyzed oxide layer of the sample oxidized at 600 °C and cooled at a cooling rate of 1 °C min^{-1} with the corresponding results of the EBSD phase analysis and the crystal orientations. It can be seen that only a few wüstite grains are present (fraction 0.03), i.e. the oxide layer consists mainly of magnetite (fraction 0.57) and hematite (fraction 0.4). The results show that the inner oxide sublayer has the smallest grain size, followed by the

Table 2 Oxide content in oxide layers of samples oxidized at high temperature (SEM EBSD analysis)

Cooling rate (°C min^{-1})	Oxidation temperature					
	600 (°C)			700 (°C)		
	Fraction of oxides			Fraction of oxides		
	Magnetite	Hematite	Wüstite	Magnetite	Hematite	Wüstite
1	0.57	0.40	0.03	0.60	0.25	0.15
10	0.27	0.68	0.05	0.44	0.40	0.16
100	0.46	0.44	0.10	0.39	0.33	0.28
1000	0.57	0.38	0.12	0.23	0.36	0.41

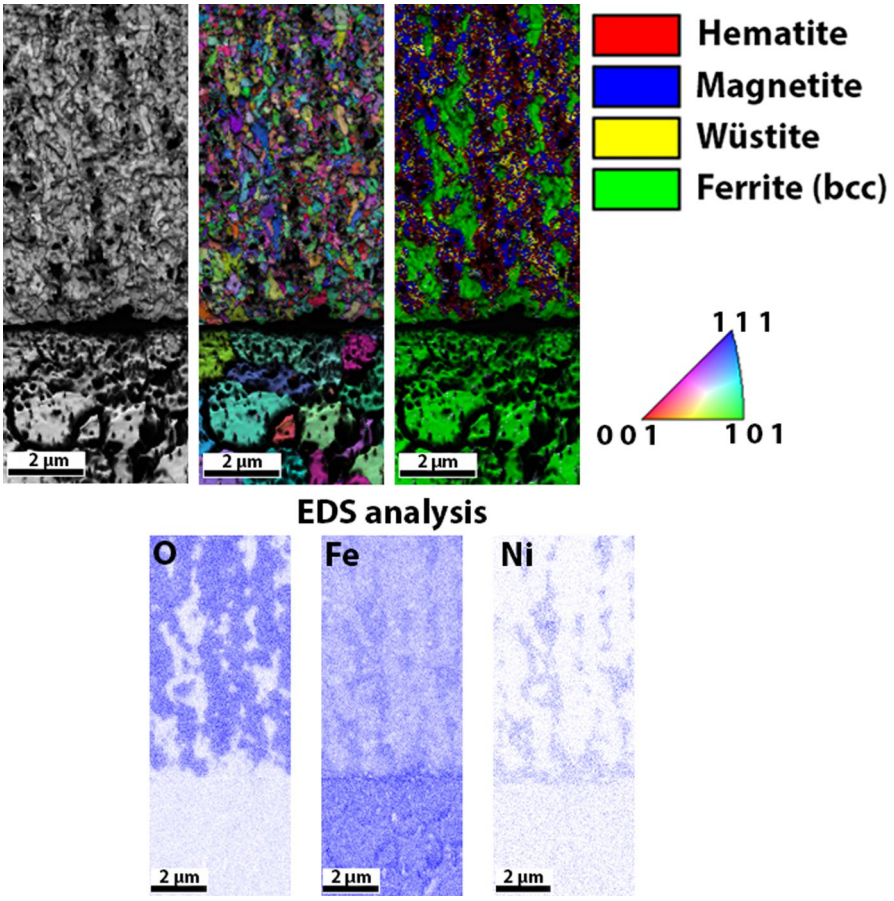

Fig. 3 SEM EBSD and SEM EDS analysis of the inner oxide sublayer (phase and element distribution) formed on the sample after high-temperature oxidation (600 °C) with a cooling rate of 1 °C min.$^{-1}$

outer oxide sublayer and the middle oxide sublayer with the largest grain size. Most of wüstite is found in the inner oxide sublayer, while the middle sublayer consists of magnetite and the outer sublayer of hematite.

Figure 5 shows an SEM image of the analyzed oxide layer of the sample oxidized at 600 °C and cooled at a cooling rate of 1000 °C min^{-1} with the corresponding results of the EBSD phase analysis and the crystal orientations. It is obvious that the fraction of wüstite increases with increasing cooling rate (fraction 0.12). Overall, the oxide layer still consists mainly of magnetite (fraction 0.57) and hematite (fraction 0.38). In this case, the fraction of magnetite is higher than that of hematite. The results show that the inner oxide sublayer has the smallest grain size, followed by the outer oxide sublayer and the middle oxide sublayer with the largest grain size. Most of the wüstite is found in the inner oxide sublayer, but in this case also in the middle sublayer, which still consists

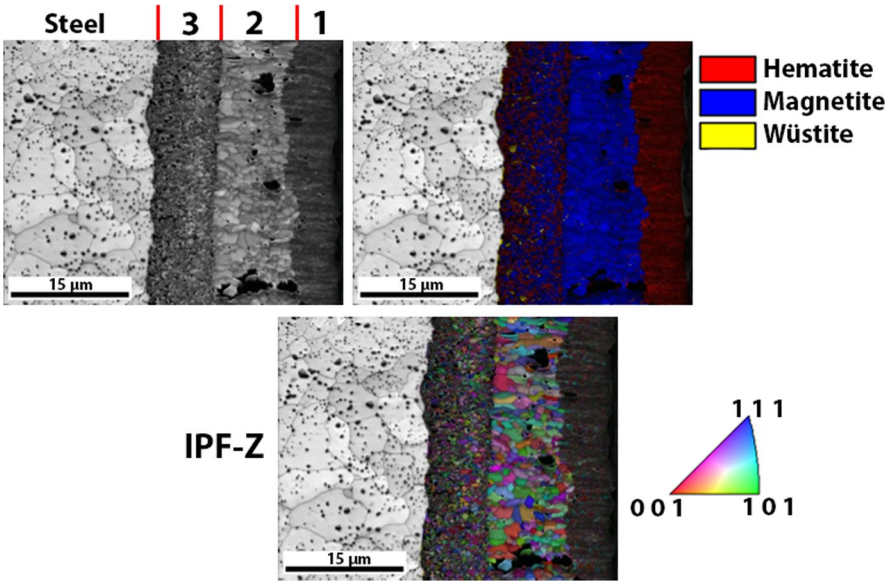

Fig. 4 SEM EBSD analysis of the oxide layer formed on the sample after high-temperature oxidation (600 °C) at a cooling rate of 1 °C min.$^{-1}$

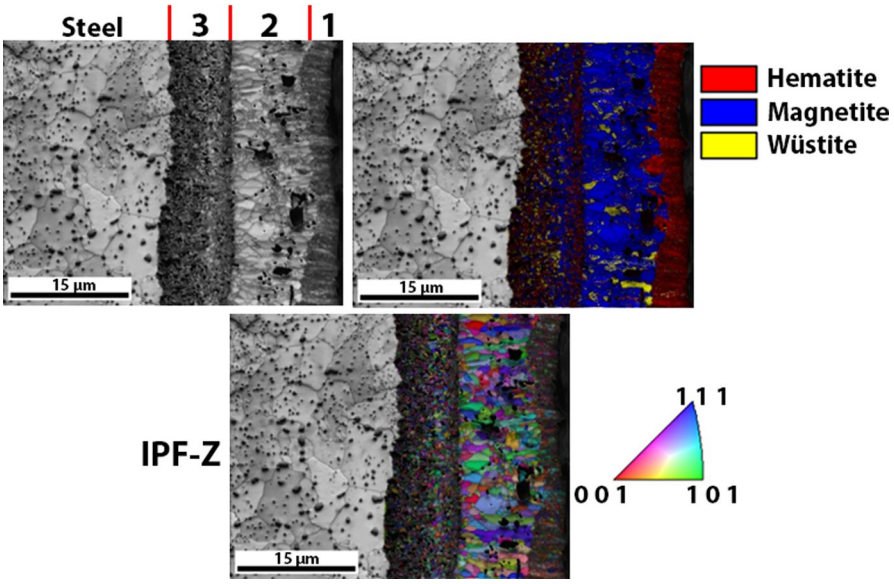

Fig. 5 SEM EBSD analysis of the oxide formed on the sample after high-temperature oxidation (600 °C) with a cooling rate of 1000 °C min.$^{-1}$

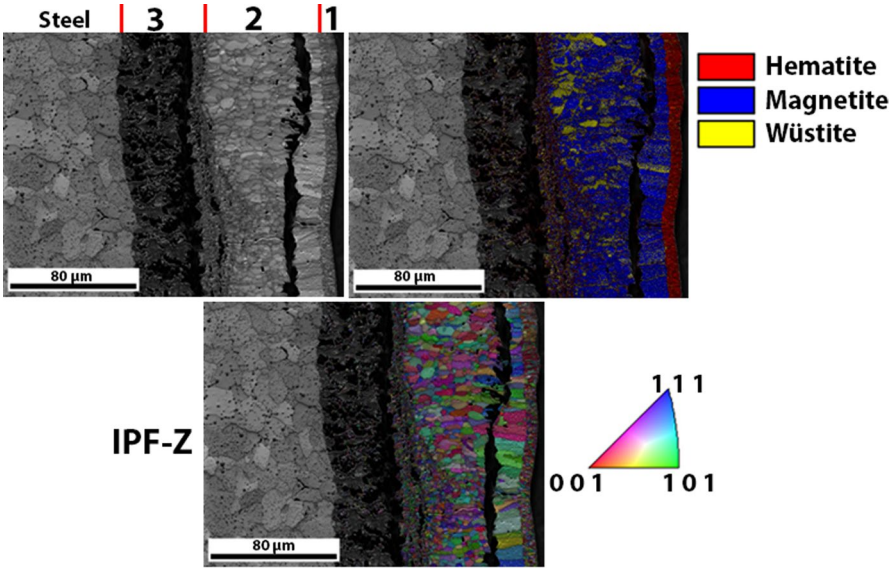

Fig. 6 SEM EBSD analysis of the oxide layer formed on the sample after high-temperature oxidation (700 °C) at a cooling rate of 1 °C min.$^{-1}$

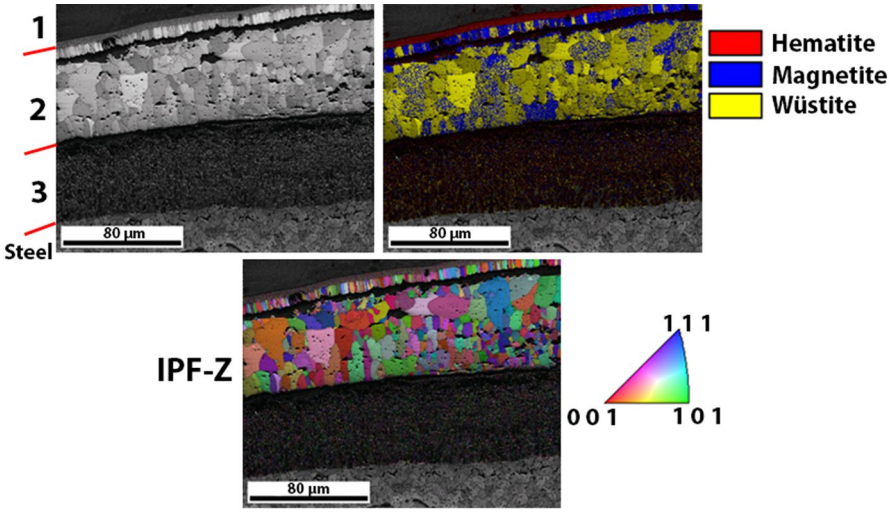

Fig. 7 SEM EBSD analysis of the oxide layer formed on the sample after high-temperature oxidation (700 °C) with a cooling rate of 1000 °C min.$^{-1}$

mainly of magnetite, and in the outer sublayer is the same as in Fig. 4 and consists of hematite.

Figure 6 shows an SEM image of the analyzed oxide layer of the sample oxidized at 700 °C and cooled at a cooling rate of 1 °C min^{-1} with the corresponding results

of the EBSD phase analysis and the crystal orientations. It is obvious that the fraction of wüstite is higher (0.15) than at 600 °C with a cooling rate of 1000 °C min^{-1} (fraction 0.12). This is the influence of the higher oxidation temperature. Overall, the oxide layer still consists mainly of magnetite (fraction 0.60) and hematite (fraction 0.25). In this case, the fraction of magnetite is higher than that of hematite. The results show that the inner oxide sublayer has the smallest grain size, followed by the outer oxide sublayer and the middle oxide sublayer with the largest grain size. In this case, wüstite is found in the inner and middle oxide sublayer, while the middle sublayer continues to consist mainly of magnetite and the outer sublayer of hematite. The difference between the results obtained at 600 °C is that in this case the proportion of wüstite in the middle oxide sublayer is higher.

Figure 7 shows an SEM image of the analyzed oxide layer of the sample oxidized at 700 °C and cooled at a cooling rate of 1000 °C min^{-1} with the corresponding results of the EBSD phase analysis and the crystal orientations. It is obvious that the fraction of wüstite has increased considerably (fraction 0.41), compared to a cooling rate of 100 °C min^{-1} (fraction 0.17), the difference is 0.24. Overall, the oxide layer also consists of magnetite (fraction 0.23) and hematite (fraction 0.36), but the proportions are lower than the proportion of wüstite. The results show that the inner oxide sublayer has the smallest grain size, followed by the outer oxide sublayer and the middle oxide sublayer with the largest grain size. In this case, wüstite is present in the inner and middle oxide sublayer, which in this case consists mainly of it, and some magnetite is still present. The outer sublayer, on the other hand, does not change during cooling or at the oxidation temperature and in all cases consists only of hematite. The difference between the results obtained at 600 °C is that in this case the proportion of wüstite in the middle oxide sublayer is higher, in this case the middle oxide sublayer consists mainly of wüstite.

Discussion

Based on the CALPHAD calculations, higher oxidation temperatures lead to a greater amount of wüstite in the oxide layer formed, especially in the inner sublayer. Thermodynamic calculations predict that the equilibrium composition of the inner oxide sublayer at 600 °C is about 40.4 wt% FeO and increases to about 72.0 wt% FeO at 700 °C. This means that a temperature increases of 100 °C approximately doubles the amount of wüstite in the inner sublayer (31.6 wt% increase). However, to reach this level, equilibrium conditions and ultra-fast cooling to room temperature are required to prevent the eutectoid transformation of wüstite.

In the current study, cooling rates of 1 °C min^{-1}, 10 °C min^{-1}, 100 °C min^{-1} and 1000 °C min^{-1} were used. Many modern oxidation experiments utilize devices such as STA and TGA that generate ASCII files of weight gain as a function of time at specific temperatures. This data facilitates kinetic studies of oxidation. Using software tools, you can mathematically analyze the experimental data and calculate reaction constants and activation energies. However, choosing the appropriate cooling rate is crucial for analyzing the composition of the oxide layer formed. Although many new devices allow the installation of modules that enable faster cooling rates,

the crucial question remains: What is the minimum cooling rate required to maintain the wüstite content observed at the oxidation temperature (above 570 °C) and suppress eutectoid transformation?

If one first compares the CALPHAD results with the experimental results, it becomes clear that the experimental fraction of wüstite does not come close to the results of the calculations. At a cooling rate of 1000 °C min^{-1}, the fraction of wüstite was 0.12 at 600 °C (0.404 CALPHAD calculations) and 0.41 at 700 °C (0.72 CALPHAD calculations). At lower temperatures the differences are larger, at higher temperatures the experimental data approach the calculated data, but the differences are still high. CALPHAD calculations assume a state of equilibrium, so this must also be taken into account. Samples of the same steel were also cooled at a cooling rate of 1800 °C min^{-1}. Most of these results have already been published [29]. In this case, the fraction of wüstite was 0.19 at 600 °C and 0.63 at 700 °C. At 600 °C there is not much difference in the fraction of wüstite, but at 700 °C the difference is (0.22) compared to the value obtained at a cooling rate of 1000 °C min^{-1}. In this case, the experimental results have approached the calculated ones with a difference of 0.09, but the difference is still significant.

Overall, it can be stated that the higher the cooling rate, the more wüstite is retained in the oxide layer, i.e. the eutectoid transformation is suppressed. The measured fractions are listed in Table 1, from which some assumptions can be derived. At an oxidation temperature of 600 °C, there is not much difference between a cooling rate of 100 °C min^{-1} and 1000 °C min^{-1}, but at 700 °C, where even the calculated wüstite fractions are higher, the cooling rates are more important. The reason for this could also be that wüstite is thermodynamically stable above 570 °C. At higher oxidation temperatures (above 700 °C), the cooling rate should therefore be at least 1000 °C min^{-1} or more. The higher it is, the higher the fraction of wüstite in the oxide layer, i.e. the eutectoid transformation is suppressed even more. For this reason, it is not useful to analyze the composition of the oxide layer of steel samples oxidized at 700 °C and above while the cooling rate was below 1000 °C min^{-1}, as the composition of the oxide layer formed does not correspond to that actually formed at the oxidized temperatures.

Conclusions

Thermodynamic calculations provide an initial insight into the composition of the oxide layer and the fraction of oxide in the oxide layer formed. Since these calculations are based on a state of equilibrium, the total fraction of each oxide present may be higher than in the experimental results. At lower temperatures the differences are greater, at higher temperatures the experimental data is closer to the calculated data. But all this also depends on the cooling rates. The higher the cooling rates, the closer the experimental results are to the calculated ones. At lower temperatures there are large differences, but at higher temperatures and cooling rates the differences decrease. As shown, the difference can be reduced to a fraction of 0.09.

With regard to the wüstite content, it is very important that the cooling rates for steel samples with an oxidation temperature of 700 °C and above are high enough

to suppress eutectoid transformation. Based on the results, this cooling rate should exceed 1000 °C min^{-1}. However, at lower temperatures (570 °C–600 °C), the cooling rate should exceed 100 °C min^{-1} to obtain the amount of wüstite that forms in the oxide layer at oxidation temperatures. Overall, the hematite and magnetite content also changes with the cooling rate, corresponding to the wüstite content.

Acknowledgements We sincerely acknowledge the support of the work by the Slovenian Research And Innovation Agency (ARIS) programs P1-0195 (B) and P2-0050 (C).

Author Contributions Conceptualization: Tilen Balaško; Methodology, formal analysis, and investigation: Tilen Balaško, Jaka Burja and Barbara Šetina Batič; Writing—original draft preparation: Tilen Balaško and Jaka Burja; Writing—review, editing and supervision: Tilen Balaško and Jaka Burja.

Data availability No datasets were generated or analysed during the current study.

Declarations

Conflict of interest The authors declare no competing interests.

References

1. Roberts G, Krauss G, Kennedy R. *Tool Steels: 5th Edition*. Materials Park, OH, USA: ASM International; 1998.
2. *ASM handbook, volume 1 : Properties and selection : irons, steels, and high-performance alloys*. Materials Park, OH: ASM International; 1990.
3. Krauss G. *Steels: Processing, Structure, and Performance*. Materials Park, OH, USA: ASM International; 2015.
4. R. A. Mesquita, *Tool steels: properties and performance*, (CRC Press, Boca Raton, FL, 2016).
5. ASM International. *Heat Treater's Guide: Practices and Procedures for Irons and Steels*. *Heat Treater's Guide: Practices and Procedures for Irons and Steels*. Metals Park, OH: ASM International; 1995.
6. TOTTEN GE. *Steel Heat Treatment: Metallurgy and Technologies: 1st Edition*. CRC Press; 2006.
7. Haidemenopoulos GN. *Physical Metallurgy: Principles and Design*. *Taylor & Francis Group, LLC*. Boca Raton, FL: CRC Press, Taylor & Francis Group; 2018.
8. P. C. Hayes, Analysis of product morphologies and reaction mechanisms on gaseous reduction of iron oxides. *Steel Res. Int.* **82**, 2011 (480–493).
9. K. Hauffe, *Oxidation of metals*, (Springer, US, New York, 1965).
10. D. J. Young, *High Temperature Oxidation and Corrosion of Metals*, (Elsevier Science, Amsterdam; Boston; London, 2016).
11. Garza-Montes-de-Oca NF. High-Temperature Oxidation. *Encycl. Iron, Steel, Their Alloy.* 2016;1720–1728.
12. N. Birks, G. H. Meier, and F. S. Pettit, *Introduction to the High Temperature Oxidation of Metals*, (Cambridge University Press, Cambridge, 2006).

13. R. Y. Chen and W. Y. D. Yeun, Review of the High-Temperature Oxidation of Iron and Carbon Steels in Air or Oxygen. *Oxid. Met.* **59**, 2003 (433–468).
14. M. H. Davies, M. T. Simnad, and C. E. Birchenall, On the Mechanism and Kinetics of the Scaling of Iron. *Jom.* **3**, 1951 (889–896).
15. J. Païdassi, The kinetics of the air oxidation of iron in the range 700–1250°C. *Acta Metall.* **6**, 1958 (184–194).
16. R. Y. Chen and W. Y. Yuen, Oxidation of low-carbon, low-silicon mild steel at 450–900°C under conditions relevant to hot-strip processing. *Oxid. Met.* **57**, 2002 (53–79).
17. Højerslev C. *Tool steels*. *Tool steels*. Roskilde: Risø National Laboratory; 2001.
18. Lin SN, Huang CC, Wu MT, Wang WL, Hsieh KC. Crucial Mechanism to the Eutectoid Transformation of Wüstite Scale on Low Carbon Steel. *Steel Res. Int.* 2017;88.
19. D. Bruce and P. Hancock, Note on the temperature stability of wüstite in surface oxide films on iron. *Br. Corros. J.* **4**, 1969 (221–222).
20. Landolt D. *Corrosion and surface chemistry of metals*. *Materials Today*. 2007.10.
21. T. J. A. Richardson, B. Cottis, R. Lindsay, et al., *Shreir's Corrosion*, vol. 1. (Elsevier Science, Elsevier Science. Amsterdam; London, 2009),.
22. L. Himmel, R. F. Mehl, and C. E. Birchenall, Self-Diffusion of Iron in Iron Oxides and The Wagner Theory of Oxidation. *JOM.* **5**, 1953 (827–843).
23. Juricic C. On the mechanisms of internal stress formation in multi-phase iron oxide scales. Ruhr University Bochum; 2009.
24. R. Y. Chen and W. Y. D. Yuen, Study of the scale structure of hot-rolled steel strip by simulated coiling and cooling. *Oxid. Met.* **53**, 2000 (539–560).
25. L. Chang and S. N. Lin, Analytical electron microscopy study of interfacial oxides formed on a hot-rolled low-carbon steel. *Oxid. Met.* **63**, 2005 (131–144).
26. H. Tanei and Y. Kondo, Effects of Initial Scale Structure on Transformation Behavior of Wüstite. *ISIJ Int.* **52**, 2012 (105–109).
27. B. Gleeson, S. M. M. Hadavi, and D. J. Young, Isothermal transformation behavior of thermally-grown wustite. *Mater. High Temp.* **17**, 2000 (311–318).
28. S. N. Lin, C. C. Huang, M. T. Wu, W. L. Wang, and K. C. Hsieh, Crucial Mechanism to the Eutectoid Transformation of Wüstite Scale on Low Carbon Steel. *Steel Res. Int.* **88**, 2017 (2–9).
29. T. Balaško, M. Vončina, J. Burja, and B. Š Batič, High - Temperature Oxidation Behavior of Tool Steel with Increased Thermal Conductivity. *Oxid. Met.* **98**, 2022 (135–161).